U.S. DEPARTMENT OF ENERGY | Office of Science

DOE/SC-ARM-TR-129

Aerosol Optical Depth Value-Added Product Report

A Koontz
G Hodges
J Barnard
E Kassianov
C Flynn
J Michalsky
E Cromwell

December 2023

ARM

DISCLAIMER

DOE/SC-ARM-TR-129

Aerosol Optical Depth Value-Added Product Report

A Koontz, Pacific Northwest National Laboratory (PNNL)
C Flynn, University of Oklahoma
G Hodges, National Oceanic and Atmospheric Administration (NOAA)
J Michalsky, NOAA
J Barnard, University of Nevada, Reno
E Cromwell, PNNL
E Kassianov, PNNL

December 2023

How to cite this document:

Koontz, A, C Flynn, G Hodges, J Michalsky, J Barnard, E Cromwell, and E Kassianov. 2023. Aerosol Optical Depth Value-Added Product Report. U.S. Department of Energy, Atmospheric Radiation Measurement user facility, Richland, Washington. DOE/SC-ARM-TR-129.

Work supported by the U.S. Department of Energy,
Office of Science, Office of Biological and Environmental Research

Acronyms and Abbreviations

AERONET	Aerosol Robotic Network
AMF	ARM Mobile Facility
AOD	aerosol optical depth
ARM	Atmospheric Radiation Measurement
CSPHOT	Cimel sunphotometer
DU	Dobson Unit
LBLRTM	line-by-line radiative transfer model
LST	Local Standard Time
LUT	look-up table
MFRSR	multifilter rotating shadowband radiometer
netCDF	Network Common Data Form
NIMFR	normal incidence multifilter radiometer
NSA	North Slope of Alaska
OMI	ozone monitoring instrument
QC	quality control
SGP	Southern Great Plains
TOA	top of atmosphere
TOD	total optical depth
TOMS	total ozone mapping spectrometer
TRACER	Tracking Aerosol Convection Interactions Experiment
VAP	value-added product

Contents

Figures

Tables

1.0 Introduction

This document describes the process applied to retrieve aerosol optical depth (AOD) from multifilter rotating shadowband radiometers (MFRSR and MFRSR7nch) and normal incidence multifilter radiometers (NIMFR and NIMFR7nch) operated at the U.S. Department of Energy Atmospheric Radiation Measurement (ARM) user facility's ground-based observatories. This value-added product (VAP) process includes:

- Routine "autonomous" (i.e., capable of being run with minimal human intervention) computation of Langley retrievals that yield first-order "V_o" calibration data
- Generation of a robust calibration time series from these first-order V_o values
- Subsequent application of this robust calibration time series to the MFRSR and NIMFR measurements
- Retrieval of optical depth at several wavelengths
- Calibration of irradiances
- Final application of an autonomous cloud screen to the aerosol AOD.

The autonomous Langley retrievals have been described in Harrison and Michalsky (1994). The generation of the robust calibration time series combines some of the techniques described in Michalsky (2001), as well as operational elements unique to the ARM deployments, to be detailed below. The cloud-screen algorithm is described in Alexandrov (2004).

The current AOD VAP and Langley VAP include modifications introduced to support the 1.6-um filter channel in the MFRSR7nch and NIMFR7nch. Specifically, the Langley calibration and calculation of AOD for this channel require filter-specific corrections for gas absorption from carbon dioxide (CO_2), methane (CH_4), and water vapor (H_2O) These modifications are described in Section 4.

2.0 Description of Algorithm

2.1 Overview

The core purpose of ARM is to reduce uncertainties in climate model predictions. A dominant source of uncertainty in these models is the radiative impact of aerosols, which has spawned a major effort in ARM to measure aerosol properties. This VAP is concerned with several important aerosol radiative properties. The most important of these is the AOD, which is a measure of the total aerosol burden in the atmosphere. The spectral dependence of AOD, typically described by the Ångström exponent, is also an indicator of particle size, with large particles having Ångström exponent values near zero and smaller particles exhibiting larger Ångström exponent values. Improved knowledge of these basic aerosol properties will help reduce the uncertainties associated with aerosol effects in climate models.

The determination of AODs and the radiometric calibration of the MFRSR and NIMFR are obtained through Langley regressions, based on linear regressions of the log of the measured irradiance versus

airmass, computed twice-daily. However, the daily Langley regressions exhibit significant noise, mostly due to atmospheric variability. To establish a stable calibration, the AOD VAP requires a period of continuous measurements long enough to reduce statistical variability below 1% per day. In practice, a two-month processing window is required at most ARM sites before it is possible to generate sufficiently stable day-to-day calibrations. After applying a stable daily calibration to the radiometric measurements, time series of total optical depths for each of five spectral channels at 415 nm, 500 nm, 615 nm, 673 nm, and 870 nm are calculated. The aerosol optical depth is then computed as the residual of the total optical depth minus the pressure-corrected Rayleigh optical depth and a satellite-derived (Total Ozone Mapping Spectrometer [TOMS] or Ozone Monitoring Instrument [OMI], depending on year) ozone optical depth. Lastly, the resulting aerosol optical depths are flagged to indicate cloud contamination on failure of a variability screen.

2.2 Langley Retrievals

Here we review the basics of the Langley regression. At a given wavelength, λ, with no clouds between the sun and the Earth's surface, the uncalibrated direct normal irradiance at the surface, $V(\lambda)$, may be described as:

$$V(\lambda) = V_0(\lambda) exp\left[-\left(\tau_{Rayleigh} + \tau_{aerosol}\right) am - \tau_{gas}(am)\right] \quad (1)$$

where:

- $V_o(\lambda)$ is the top-of-atmosphere irradiance (known colloquially as "V-naught") with units of "counts" (actually the output voltage of the instrument after an analog-to-digital conversion)
- am is the airmass
- $\tau_{gas}(am)$ is the gas absorption as a function of airmass
- $\tau_{Rayleigh}$ is the Rayleigh optical depth due to molecular scattering
- $\tau_{aerosol}$ is the AOD.

Note that the airmass is the amount of atmosphere between the sun and the surface, normalized such that the airmass is equal to one when the sun is directly overhead. Given the time of day and the site's latitude and longitude, the airmass is easily calculated using the formula of Kasten and Young (1989):

$$am = 1.0 / [\cos(Z) + 0.50572 \times (96.07995 - Z)^{-1.6364}] \quad (2)$$

where Z is the solar zenith angle.

For many, but not all, parts of the solar spectrum, gas absorption is negligible, or the absorption is linearly proportional to the airmass. For these spectral regions, the above equation becomes:

$$V(\lambda) = V_0(\lambda) exp\left[-\left(\tau_{Rayleigh} + \tau_{aerosol} + \tau_{gas}\right) am\right] \quad (3)$$

In the above equation, τ_{gas} may be zero, or so close to zero as to be negligible.

Taking the natural logarithm of each side gives:

$$log[V(\lambda)] = log[\,V_0(\lambda)] \; - \left(\tau_{Rayleigh} + \tau_{aerosol} \; + \tau_{gas}\right)am \qquad (4)$$

This equation represents the essence of the Langley regression. The slope of this line is the total optical depth (TOD), defined as $\tau_{Rayleigh} + \tau_{aerosol} + \tau_{gas}$, and the y-intercept is the $log[V_o(\lambda)]$. Figure 1 illustrates this concept, using MFRSR measurements of direct normal irradiance.

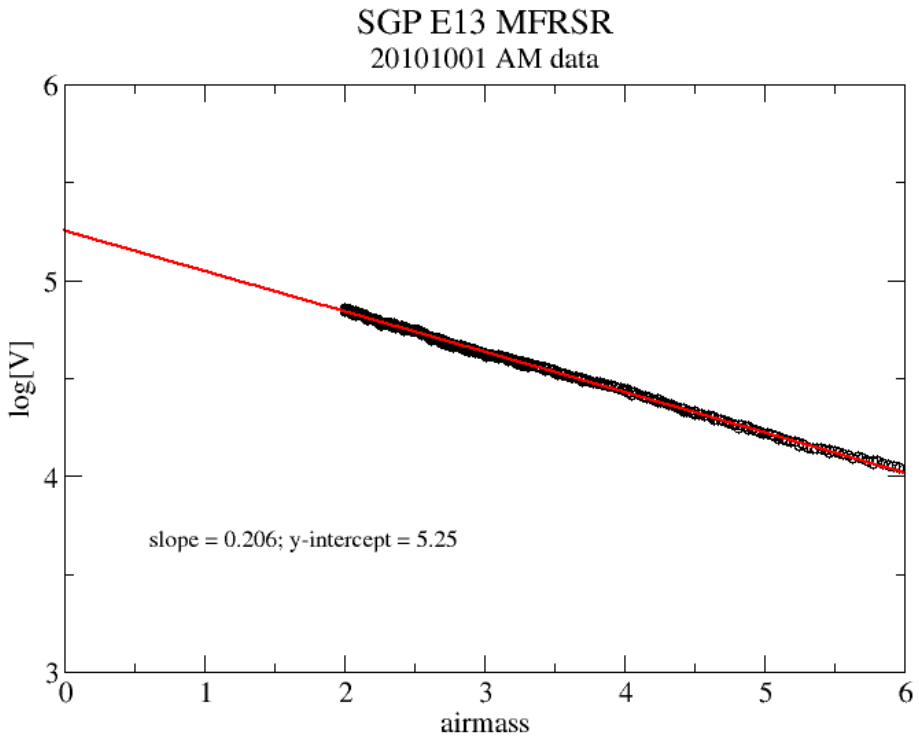

Figure 1. Illustration of a Langley regression. The data for this regression, represented by the black dots, are taken from the Southern Great Plains (SGP) E13 facility's MFRSR on October 1, 2010, in the morning. The wavelength is 500 nm. The red line indicates a linear fit to these data. The slope of the line, 0.206, is the total optical depth. The y-intercept is log[V_o].

The Langley VAP uses MFRSR or NIMFR data and produces a V_o value for two distinct periods during daylight hours. The first period is for morning hours, for airmass values between 6 and 2; the second period is for afternoon hours, for airmass values between 2 and 6. In addition, each Langley regression is deemed "good" or "bad". The primary cause of a poor Langley regression is cloud contamination. Although the algorithm attempts to remove cloud contamination, some residual contamination may be present that would unacceptably increase the uncertainty of the linear fit. If the uncertainty is too large, for whatever the cause, these "bad" Langley events are discarded. Additionally, for days with completely overcast conditions, a Langley regression is not possible.

Even when the noisiest Langley events are thrown out, the good V_o are still subject to random noise. Perhaps the leading cause of this random noise is the variation of the AOD during the time that the Langley regression takes place. Marenco (2007) demonstrates that a Langley regression can appear quite

linear, and therefore "good", even when significant aerosol variation occurs. This variation may introduce significant noise in derived V_o values. The basic premise of the AOD VAP is to obtain as much Langley V_o data as possible, both before and after the date of interest, and then filter these data to reduce the effect of noise sources discussed above.

We note here that all the V_o values illustrated in Figure 2 have been corrected for the eccentricity of the Earth's orbit that occurs during a year. During the winter months, the sun is closer to the Earth, and vice versa during the summer months. This orbital variation results in measured irradiance variations of about ± 3%, and this variation would show up as a "sine wave" in these data with a period of exactly one year, peaking in the winter, when the Earth is closest to the sun, and vice versa for the summer.

2.3 Obtaining Robust Daily Calibrations

Referring to Figure 2, let's now look at a time series of good V_os. This time series is taken over a year using data from the SGP E13 MFRSR. The V_os are indicated by the blue circles. Over the year 2010, 293 Langley events occurred that were deemed good. Figure 2 shows that there is considerable noise of about ±10%, even when only considering the good Langley events. This noise must be filtered out. Filtered, "correct" V_os for each day of the year are indicated by the red curve in Figure 2. Henceforth, we shall refer to the filtered V_os as $V_{o,f}$. To calculate $V_{o,f}$ values we follow a method described by Forgan (1988, 1994).

This technique consists of a three-step process. The first of these is to form a ratio of V_os from two wavelength channels, 415 and 870 nm; this ratio is thought to exhibit less variability than the raw V_os (see Forgan 1988). Second, we apply a sliding window (analogous to the well-known "boxcar" filter) of two-month length to the ratio time series. As the window slides along in time, we remove all ratios in the lower and upper 25% quartiles, leaving half of the original points. The underlying assumption here is that this pruning of points acts as a filter, eliminating outliers; we are then left with a time series of V_os with considerably less noise. The third step takes our pruned time series and smooths it using a Gaussian filter of 30-day width; from this we get a $V_{o,f}$ value for a time corresponding to the center of the sliding window as illustrated by the red curve in Figure 2. This curve provides daily $V_{o,f}$ values for any time of interest, except close to the times when the instrument hardware is changed—a special situation that will be discussed below.

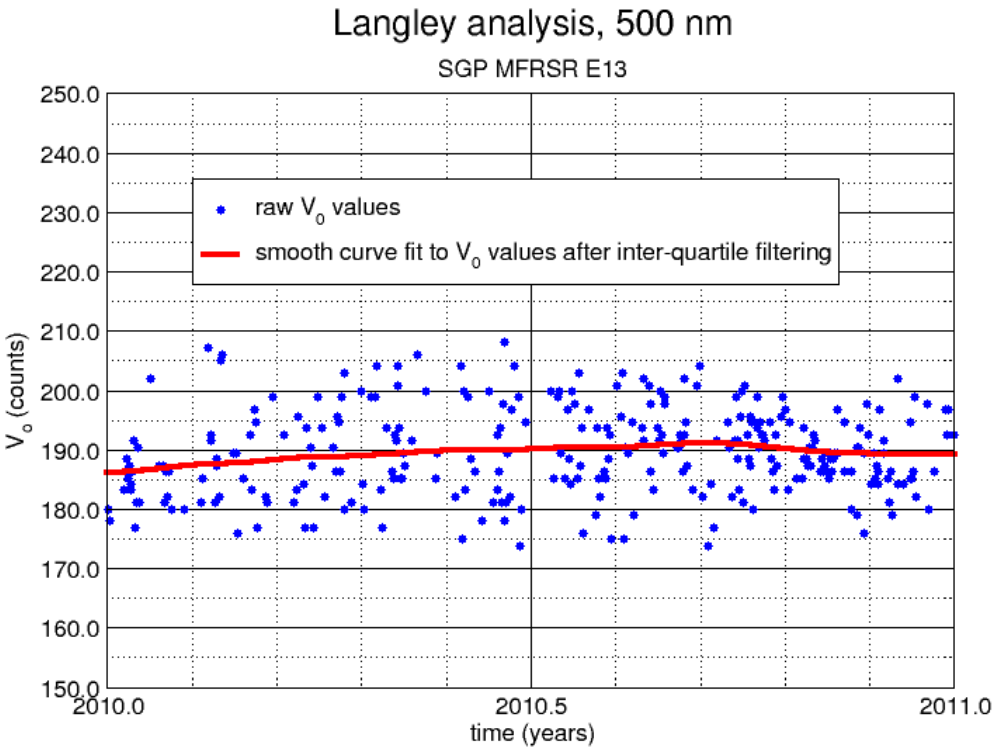

Figure 2. Time series of V_os (blue dots) from the SGP E13 MFRSR. The red line is a smooth curve fit to these data, from which daily corrected $V_{o,f}$ values may be obtained. In this figure, all values have been corrected for the eccentricity of the Earth's orbit.

2.4 Computing Total and Aerosol Optical Depths

With daily $V_{o,f}$s in hand, it is a trivial matter to calculate TODs by rearranging Equation 4 to become

$$TOD(t) = \left(\tau_{Rayleigh} + \tau_{aerosol+}\tau_{gas}\right) = -\frac{1}{am}\log\left[\frac{V(\lambda,t)}{V_{0,f}(\lambda)}\right] \quad (5)$$

We note two things about this seemingly simple equation. First, we can calculate TOD during any time of the day, given a daily $V_{o,f}$ value for that day; the output of the MFRSR, $V(\lambda,t)$ at time, t; and an absence of clouds between the MFRSR and the sun. Second, we must know the gas absorption, τ_{gas}. For many regions of the solar spectrum, τ_{gas} is effectively zero. However, ozone absorption is important for the MFRSR and NIMFR 500-, 615-, and 673-nm wavelength channels and must be accounted for. These wavelengths, particularly 615 nm, are significantly influenced by ozone absorption in the Chappuis band (Goody and Yung 1989). We denote the gas absorption from ozone as τ_{ozone}. Third, the Rayleigh (molecular) optical thickness, $\tau_{Rayleigh}$, must be calculated.

Finding the ozone optical depth for the appropriate channels is also straightforward if we have an estimate of the columnar amount of ozone. For this value, we use data from the TOMS (http://science.nasa.gov/missions/toms/) or the OMI (http://aura.gsfc.nasa.gov/instruments/omi.html);

these data have been stored in the ARM Data Center from July 25, 1996 to the present. (In the Data Center, the datastream is named gecomiX1.a1). Using the latitude and longitude at which the MFRSR or NIMFR instrument is physically located, we determine a suitable ozone value by an interpolation technique. If no ozone data is available for a particular day, a site-specific default value is used. Once we have a columnar value of ozone (with the rather arcane units of "atmosphere-centimeter" [atm-cm], which are equal to one Dobson Unit divided by 1000, http://ozonewatch.gsfc.nasa.gov/), we find τ_{ozone} as

$$\tau_{ozone}(\lambda) = (Columnar\ ozone, atm.cm) * A_{ozone}(\lambda) \quad (6)$$

where "Columnar ozone, atm-cm" is the amount of ozone in the atmospheric column and Aozone(λ) is the ozone gas absorption coefficient – a function of wavelength. For the Chappuis band, the absorption coefficients are listed in Appendix A.

Given the surface pressure, determining $\tau_{Rayleigh}$ is found using the formula (Hansen and Travis 1974):

$$\tau_{Rayleigh} = \frac{p}{1013.25} 0.008569\lambda^{-4}(1 + 0.0133\lambda^{-2} + 0.00013\lambda^{-4}) \quad (7)$$

where p is the surface pressure in millibars.

The top panel in Figure 3 shows a typical AOD time series obtained from the SGP E13 MFRSR for the date October 2, 2010. The AODs are shown for the five wavelengths at which AODs may be calculated: 415, 500, 615, 673, and 870 nm. It is not possible to find AODs using the Langley method at 940 nm because this channel is contaminated by water vapor (the 940-nm channel is used to retrieve columnar abundances of water vapor). The AODs for this particular day are quite low; for 500 nm the average AOD is about 0.04. The estimated error of AODs obtained from the technique described above is ± 0.01. However, some of the plotted AODs are contaminated by cloud and need to be removed; see, for example, the data just after 1400 hours, local standard time (LST). This removal will be discussed below.

Calculation of the aerosol Ångström exponent is done using the 415- and 870-nm wavelengths, and follows the well-known Ångström relation

$$\tau_{aerosol}(\lambda) = A\lambda^{-n} \quad (8)$$

where A is a constant and n is the Ångström exponent. Applying this relationship to find n using the two wavelengths specified above gives this formula

$$n = -log\left[\frac{\tau_{aerosol}(\lambda = 415\ nm)}{\tau_{aerosol}(\lambda = 870\ nm)}\right] \Big/ log\left[\frac{415}{870}\right] \quad (9)$$

The bottom panel of Figure 3 shows the Ångström exponent calculated from the optical depths shown in the top panel.

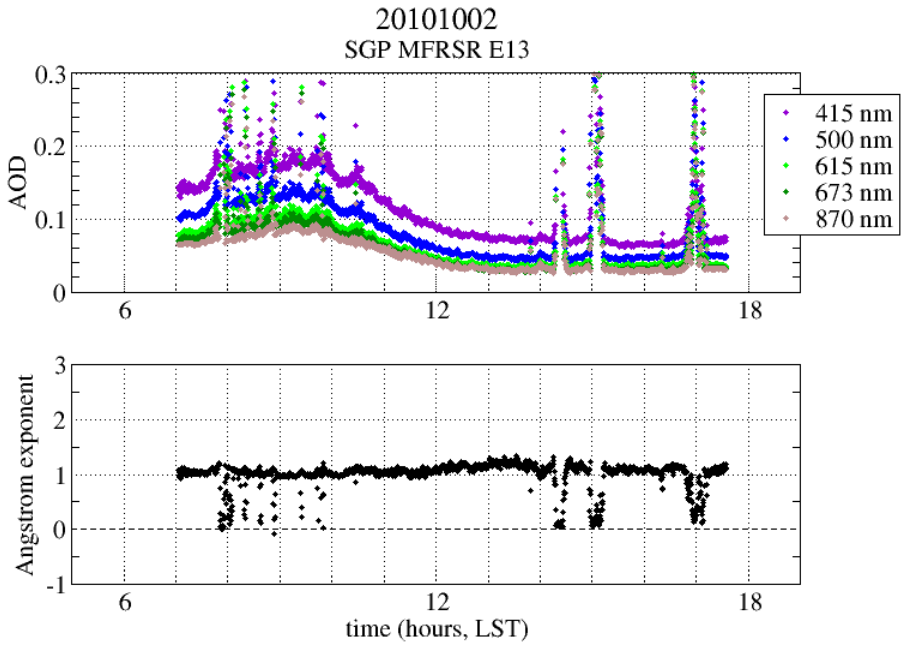

Figure 3. The top panel shows a time series of AOD for five MFRSR wavelengths. The cloud screen has not been applied. The bottom panel displays the Ångström exponent.

2.5 Application of a Cloud Screen

During this day, cloud contamination of AOD is evident at times when the AOD turns up sharply and is seen multiple times in Figure 3. We remove these erroneous AODs from the time series through a procedure we call "cloud screening". This screening is based on the algorithm of Alexandrov et al. (2004). Briefly, this algorithm examines the variability of an AOD time series. If the variability is small over a specified time interval, the AODs are assumed to be good. Otherwise, they are rejected. The demarcation between accepted and rejected AODs is a specified parameter–the so-called "threshold value"–is determined by both quantitative and visual analysis. The parameter is adjusted to be conservative; that is, it tends to identify some AODs as being contaminated, when in fact they are not, thereby embracing the idea that it is better to err on the side of removing a few good AODs rather than letting a significant number of cloud-contaminated AODs slip through. Figure 4 shows the cloud screen applied to the 500-nm channel shown in Figure 3. The blue dots in Figure 4 are the AODs that have been screened, whereas the red dots show AODs that are likely to be cloud-contaminated.

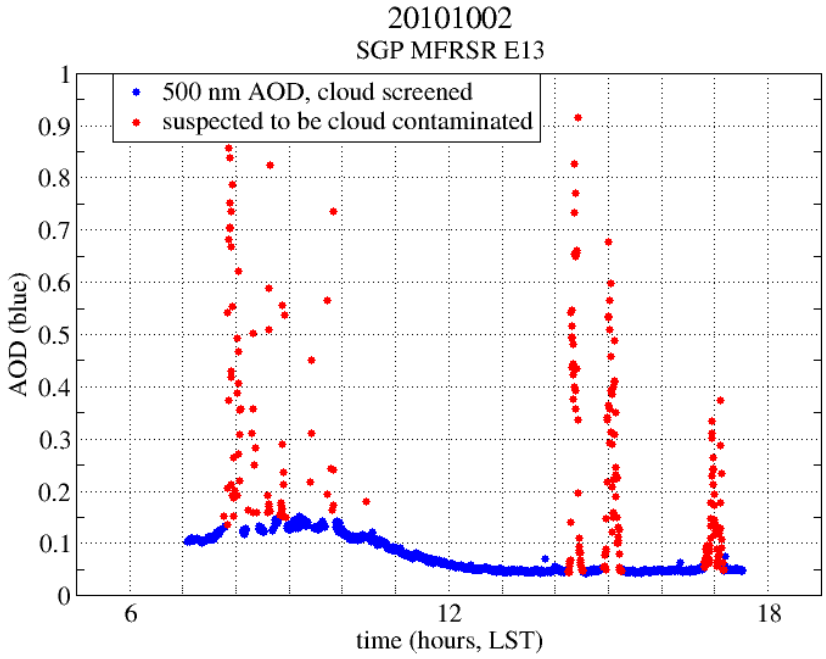

Figure 4. Illustration of the cloud screening technique, applied to the 500-nm wavelength channel shown in Figure 3. The blue circles represent AODs that have been screened and are unlikely to be contaminated by cloud.

2.6 Calibration of Irradiances to Top-of-Atmosphere Values

The initial, nominal calibration of MFRSR irradiances is done using a standard lamp (Keidron et al. 1999; see also http://www.arm.gov/publications/tech_reports/handbooks/mfr_handbook.pdf). These calibrations can be improved upon by using the results of the Langley technique and a measured composite "top-of-atmosphere" (TOA) extraterrestrial spectrum. Such a spectrum, known as the Gueymard spectrum (2004), is shown in Figure 5. For 500 nm, over a typical filter passband of about 10 nm, the value of the TOA irradiance is 1.963 $W/m^2/nm$. (A "passband" is the actual spectral width of an interference filter used in MFRSRs and NIMFRs. For a nominal wavelength of 500 nm, an MFRSR actually measures irradiances from about 495 nm to 505 nm.)

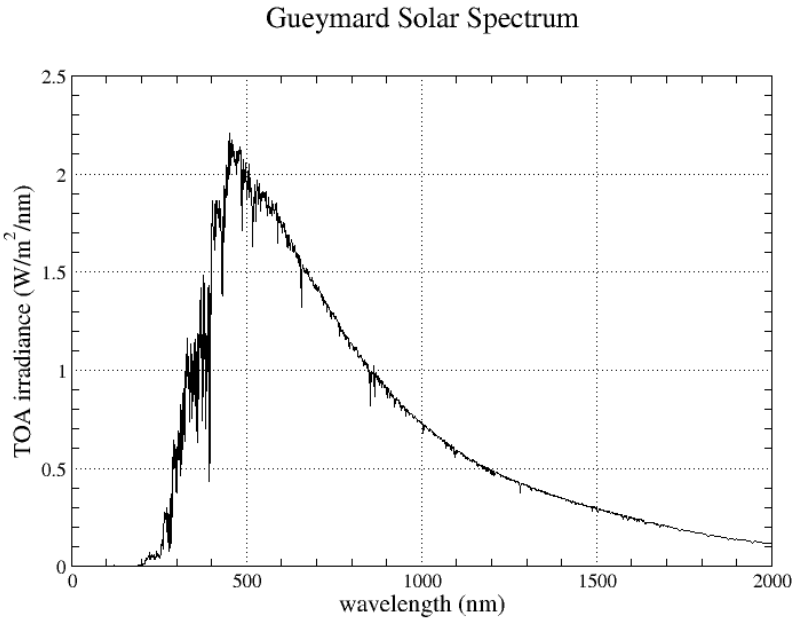

Figure 5. Top-of-atmosphere solar spectrum, which may be used to calibrate MFRSR or NIMFR irradiances.

We calibrate the MFRSR irradiances so that Vo_f is equal to the corresponding TOA value, thereby producing a time-dependent scale factor, $C(\lambda,t)$:

$$C(\lambda, t) = TOA(\lambda)/V_{o,f}(\lambda, t) \quad (10)$$

where $TOA(\lambda)$ is the TOA spectrum at the wavelength λ, integrated over the MFRSR/NIMFR passband. Note that this "pegging" of irradiances to a TOA spectrum can only occur for the wavelengths at which Langley regressions are possible: 415, 500, 615, 673, and 870 nm. For the 940-nm channel, we must rely on the standard lamp calibration. Figure 6 shows MFRSR irradiances corrected using TOA values.

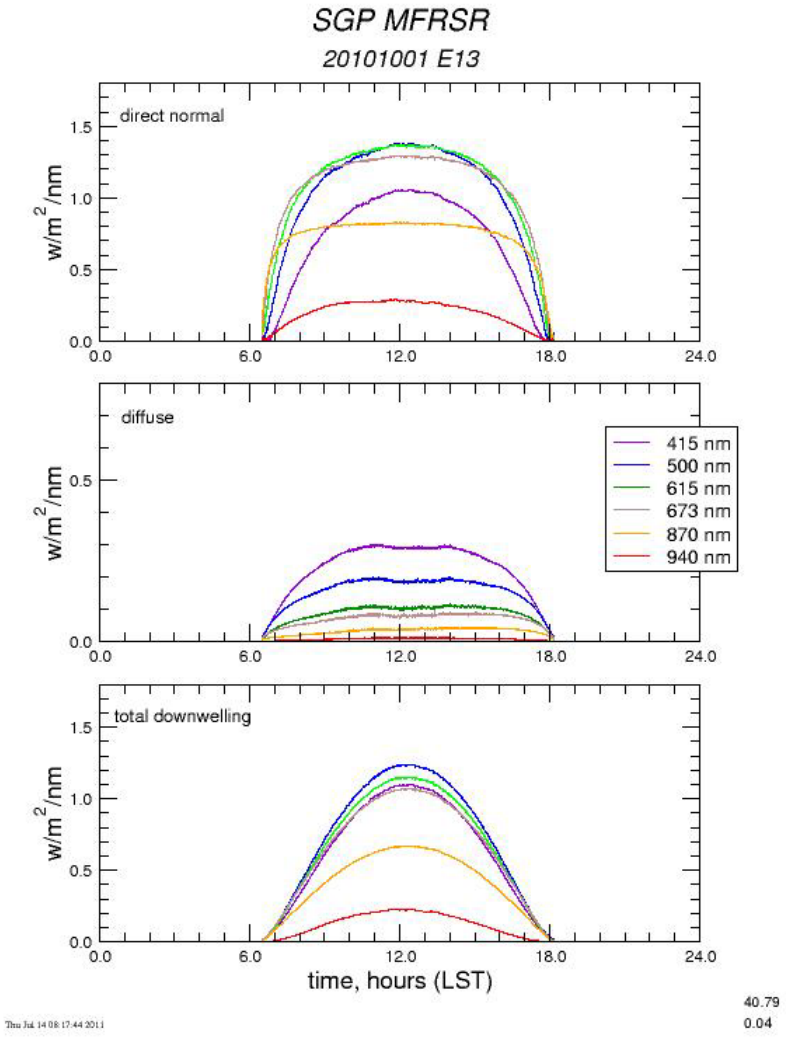

Figure 6. All three components (direct, diffuse, and total) of the solar irradiance, calibrated to TOA values using the Langley method. For the 940-nm channel, we must rely on a standard lamp calibration.

3.0 Algorithm Technical Considerations

3.1 Change of Hardware

At the time of an MFRSR hardware change, a discontinuity may be introduced into the calibration process. This discontinuity stems from the fact that the nominal calibration of MFRSR sensors differs between sensors, therefore causing an abrupt step up or step down in V_o values precisely at the time that the hardware change takes place. The sliding window method, described above, cannot be applied over the boundaries where this step change occurs. In these situations, one edge of the sliding window, of an approximately 60-day width, is allowed to butt up against the step change, and the smoothed value at the middle of window is used as the V_o value from this point to the time of the calibration change.

3.2 VAP Output

The output from the AOD VAP is a netCDF file. These files are named, for example, sgpmfrsraod1michC1.c1 and sgpnimfraod1michC1.c1 for the MFRSR and NIMFR, respectively, at the SGP C1 site. Refer to Appendix B for the structure of these netCDF files. In this Appendix, filter1 through filter5 refer to the 415-, 500-, 615-, 673-, and 870-nm wavelength channels.

3.3 Running the VAP (Command Line Arguments)

The typical command line, with options, is:

mfrod1barnmich -f sgp.C1.b1 -p mfrsr -d 20010502

where -f is defined as follows:

sss.Fn.b1

sss is the site identifier, such as:

"sgp" for Southern Great Plains

"nsa" for North Slope of Alaska

Fn is the facility identifier, such as "C1" or "M1"

Thus, a typical –f option would be: –f sgp.C1.b1, nsa.C1.b1, twp.C3.b1, or pvc.M1.b1

"-p mfrsr" specifies using the MFRSR data as input

"-p nimfr" specifies use of the NIMFR data as input

"-Z", if present, specifies skipping the Forgan technique and requires use of a text file containing daily Vo values, as described below.

"-d 20010502" specifies for which date to generate optical depth data (and the date for which to look for input data). The format of the date entry is YYYYMMDD, where "YYYY" is a four-digit representation of the year, "MM" is a two-digit representation of the month, and "DD" is a two-digit representation of the day of the month.

We currently run the AOD VAP on all sites for which we have an MFRSR or NIMFR instrument. Most ARM Mobile Facility (AMF) sites pose a challenge because obtaining sufficient good V_os is difficult. In those cases, we manually obtain V_o values for each day of the AMF deployment and place those V_o values in a site-specific text file. The AOD VAP is then executed with a special command line option, which uses the V_o values in the text file instead of using the Forgan technique described above. See the –Z command line option above.

3.4 Data Quality Assessment Included

A "variability_flag" field contains a value close to zero (0) during times of relatively stable optical depth. That is, the sliding window algorithm included in this VAP has checked the temporal stability of the

computed optical depths. When the optical depths vary widely from one sample to the next, this stability flag will be set to one (1). This may indicate that clouds were present, for example.

Most measured variables are accompanied with data quality flags, based on various criteria. For example, we attempt to flag variables that are far outside physically plausible limits. We set quality control (QC) bits based on these checks. In most cases, if a QC bit is non-zero, this indicates a possible problem with the data for a particular field. The data user is advised to carefully examine the various QC values and the underlying reasons for a particular QC bit being set.

4.0 Gas Absorption Corrections

The new MFRSR seventh channel has a nominal wavelength (λ_0) of 1625-nm and passband of about 20 nm with non-uniform filter envelope $T_{filter}(\lambda)$ (Figure 7). In other words, the MFRSR measures irradiances unevenly from about 1605-nm to 1645-nm wavelength. Absorption spectra of carbon dioxide (CO_2), methane (CH_4), and water vapor (H_2O) depend strongly on wavelength within the spectral range (1605-1645 nm) (Figure 7). Therefore, accurate calculations of average gas absorptions ($\overline{\tau_{CO_2}}$, $\overline{\tau_{CH_4}}$, and $\overline{\tau_{H_2O}}$) over a given filter envelope $T_{filter}(\lambda)$ are paramount when it comes to use slightly modified versions of Equation (3) and Equation (5) for the new channel. It should be mentioned that both the molecular (or Rayleigh) scattering coefficient and the aerosol extinction coefficient have weak spectral dependence within this spectral range (1605-1645 nm). Thus, the corresponding values of these coefficients at the nominal wavelength are used for calculations of the corresponding values of optical depth ($\tau_{Rayleigh}$, $\tau_{aerosol}$) (see Equation (3) and Equation (5)).

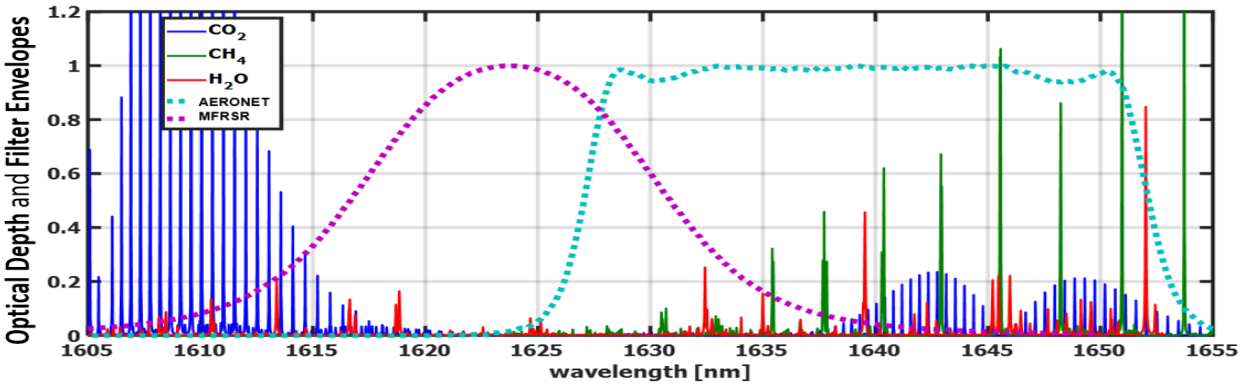

Figure 7. Optical depth spectra of carbon dioxide (blue), methane (green), water vapor (red), and filter envelopes for the MFRSR seventh channel (magenta, dashed) and AERONET Cimel sunphotometer (CSPHOT; light blue, dashed) near 1600-nm wavelength.

To calculate $\overline{\tau_{CO_2}}$ and $\overline{\tau_{CH_4}}$ for a given airmass am, a three-step approach is applied. First, spectral gas transmittance $T_{gas}(\lambda) = exp\left(-\tau_{gas}(\lambda)am\right)$ is computed using line-by-line radiative transfer model (LBLRTM; Clough et al., 2005). Here, the subscript "gas" defines either CO_2 or CH_4. Second, the computed transmittance convolving with the filter envelope gives the average transmittance

$$\overline{T_{gas}} = \int T_{gas}(\lambda)\, T_{filter}(\lambda)\, d\lambda \tag{11}$$

Finally, the corresponding average gas absorption is calculated by taking the natural logarithm of $\overline{T_{gas}}$ and dividing it by am

$$\overline{\tau_{gas}} = -ln\left(\overline{T_{gas}}\right)/am \tag{12}$$

The LBLRTM-based calculations of $\overline{\tau_{gas}}$ are computationally time consuming. Thus, these calculations have been performed once over the expected range of am (from 1 to 6) to generate the corresponding look-up tables (LUT). Then, the generated LUTs are used to parameterize the average gas absorption as a second-order polynomial function

$$\overline{\tau_{gas}} = A_{gas} + B_{gas}am + C_{gas}am^2 \tag{13}$$

The polynomial coefficients (Equation 13) are saved in netCDF attributes (for both CO_2 and CH_4).

To calculate $\overline{\tau_{H_2O}}$ for a given precipitable water vapor (pwv), the three-step approach outlined above is applied as well with a minor modification: pwv is used instead of am. Recall, pwv defines the vertically integrated amount of water vapor in the atmosphere and pwv is available at the ARM sites from complementary measurements. The calculations of $\overline{\tau_{H_2O}}$ have been performed over the expected range of pwv (from 1 to 10 cm) to generate the corresponding LUTs. Then, the generated LUTs are used to parameterize the average absorption as a second-order polynomial function

$$\overline{\tau_{H_2O}} = exp\left(A_{H_2O} + B_{H_2O}pwv + C_{H_2O}pwv^2\right) \tag{14}$$

The polynomial coefficients (Equation 14) are saved in netCDF attribute (HO_2).

Recall, Equation (3) represents monochromatic measurements for a given wavelength where gas absorption is negligible. Narrowband counterpart of Equation (1) accounts for gas absorption

$$\overline{V_n}(\lambda_0) = \overline{V_0}(\lambda_0)\, exp\left[-\left(\tau_{Rayleigh}(\lambda_0) + \tau_{aerosol}(\lambda_0)\right) am\right], \tag{15}$$

where $\overline{V_n}(\lambda_0) = \overline{V}(\lambda_0)/\overline{T_{CO_2}}\,\overline{T_{CH_4}}\,\overline{T_{H_2O}}$ is the uncalibrated direct normal irradiance at the surface normalized (subscript "*n*") by the product of the average gas transmittances calculated for a given am and pwv. Such normalization allows one to remove potential impacts of three gases considered here (carbon dioxide, methane, water vapor) on the estimation of the top-of-atmosphere narrowband irradiance $\overline{V_0}(\lambda_0)$ as the intercept of the Langley regression (Section 2.2).

Similarly, Equation (5) represents monochromatic measurements at a given time (*t*) and for a given wavelength where gas absorption is negligible. The narrowband counterpart of Equation (5) accounts for gas absorption and provides aerosol optical depth corrected for gas absorption

$$\tau_{aerosol}(t) = TOD(t) - \tau_{Rayleigh}(t) - \left(\overline{\tau_{CO_2}}(t) + \overline{\tau_{CH_4}}(t) + \overline{\tau_{H_2O}}(t)\right), \tag{16}$$

where

$$TOD(t) = -\,ln\left[\overline{V}(\lambda_0, t)/V_{o,f}(\lambda_0)\right]/am, \tag{17}$$

The daily value $V_{o,f}(\lambda_0)$ is obtained for a day of interest from the robust daily calibrations (Section 2.3).

The MFRSR AOD calculated for the new channel using Equation (16) is compared with Aerosol Robotic Network (AERONET) AOD obtained from collocated and coincident measurements at 1640-nm wavelength (Giles et al. 2019) during the recent ARM-supported Tracking Aerosol Convection Interactions Experiment (TRACER; Houston, Texas). The comparison results in Figure 8 demonstrate that the MFRSR AOD (1625 nm) is in a good agreement with the AERONET AOD (1640 nm) despite the strong both diurnal and day-to-day changes of aerosol loading occurred during the TRACER campaign.

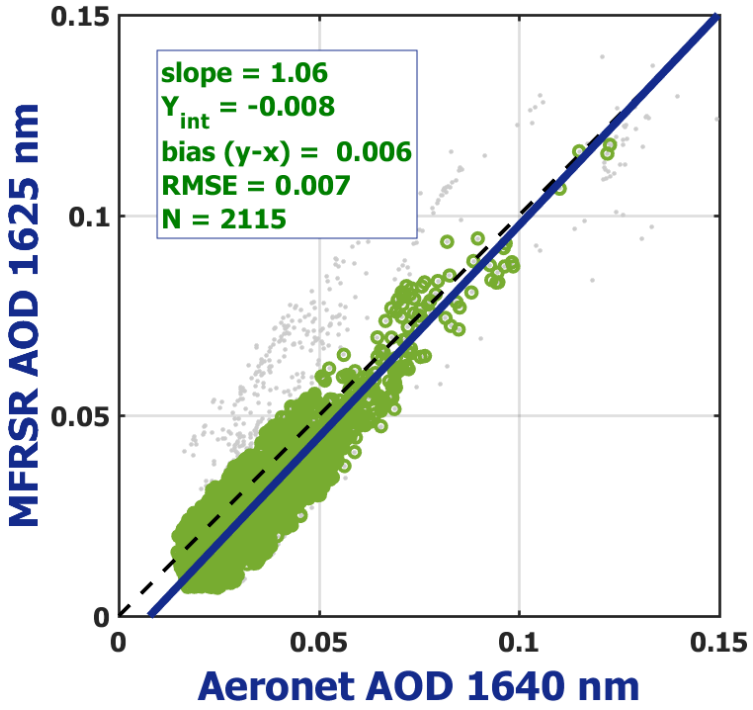

Figure 8. Comparison of the MFRSR AOD (1625 nm) with AERONET AOD (1640 nm) during TRACER. The short-dashed line is the 1:1 correspondence line and the solid line is the linear regression. Points with light gray color represent statistical outliers excluded from the fitting process. The basic statistics of the comparison are included as well.

5.0 Summary

The AOD VAP computes optical depth and related values, using output of the Langley VAP, as well as either MFRSR or NIMFR data as input. This document has described the details about both the Langley VAP and the AOD VAP and their modifications introduced recently to support the 1.6-um filter channel in the MFRSR7nch and NIMFR7nch data. For a relatively up-to-date description of MFRSR performance over a long period, the reader is urged to consult Michalsky and LeBaron (2013). This paper discusses data obtained from an MFRSR that has run more or less continuously in the Salt Lake City area for 15 years, and in particular, it describes degradation of cosine response with time and how this might be corrected.

6.0 References

Alexandrov, M, A Marshak, B Cairns, A Lacis, and B Carlson. 2004. "Automated cloud screening algorithm for MFRSR data." *Geophysical Research Letters* 31(4): L04118, https://doi.org/10.1029/2003GL019105

Clough, SA, MW Shephard, EJ Mlawer, JS Delamere, MJ Iacono, K Cady-Pereira, S Boukabara, and PD Brown. 2005. "Atmospheric radiative transfer modeling: A summary of the AER codes." *Journal of Quantitative Spectroscopy & Radiative Transfer* 91(2): 233–244, https://doi.org/10.1016/j.jqsrt.2004.05.058

Forgan, BW. 1986. "Sun photometer calibration by the ratio-Langley method." In *Baseline Atmospheric Program*. Edited by BW Forgan and PJ Fraser, pp. 22-26. Bureau of Meteorology, Melbourne, Australia.

Forgan, BW. 1994. "General method for calibrating Sun photometers." *Applied Optics* 33(21): 4841–4850, https://doi.org/10.1364/AO.33.004841

Giles, DM, A Sinyuk, MG Sorokin, JS Schafer, A Smirnov, I Slutsker, TF Eck, BN Holben, JR Lewis, JR Campbell, EJ Welton, SV Korkin, and AI Lyapustin. 2019. "Advancements in the Aerosol Robotic Network (AERONET) Version 3 database – automated near-real-time quality control algorithm with improved cloud screening for Sun photometer aerosol optical depth (AOD) measurements." *Atmospheric Measurement Techniques* 12(1): 169–209, https://doi.org/10.5194/amt-12-169-2019

Goody, RM and YL Yung. 1989. *Atmospheric Radiation: Theoretical Basis*. Oxford University Press, New York.

Gueymard, C. 2004. "The Sun's total and spectral irradiance for solar energy applications and solar radiation models." *Solar Energy* 76(4): 423–453, https://doi.org/10.1016/j.solener.2003.08.039

Hansen, J, and L Travis. 1974. "Light scattering in planetary atmospheres." *Space Science Reviews* 16: 527–610, https://doi.org/10.1007/BF00168069

Harrison, L, and J Michalsky. 1994. "Objective algorithms for the retrieval of optical depths from ground-based measurements." *Applied Optics* 33(22): 5126–5132, https://doi.org/10.1364/AO.33.005126

Kasten, F, and A Young. 1989. "Revised optical air mass tables and approximation formula." *Applied Optics* 28(22): 4735–4738, https://doi.org/10.1364/AO.28.004735

Kiedron, P, J Michalsky, J Berndt, and L Harrison. 1999. "Comparison of spectral irradiance standards used to calibrate shortwave radiometers and spectroradiometers." *Applied Optics* 38(12): 2432–2439, https://doi.org/10.1364/AO.38.002432

Marenco, F. 2007. "On Langley plots in the presence of a systematic diurnal aerosol cycle centered at noon: A comment on recently proposed methodologies." *Journal of Geophysical Research – Atmospheres* 112(D6): D06205, https://doi.org/10.1029/2006JD007248

Michalsky, JJ, J Schlemmer, W Berkheiser, J Berndt, L Harrison, N Laulainen, N Larson, and J Barnard. 2001. "Multiyear measurements of aerosol optical depth in the Atmospheric Radiation Measurement and Quantitative Links programs." *Journal of Geophysical Research – Atmospheres* 106(D11): 12,099–12,107, https://doi.org/10.1029/2001JD900096

Michalsky, JJ, and B LeBaron. 2013. "Fifteen-year aerosol optical depth climatology for Salt Lake City." *Journal of Geophysical Research – Atmospheres* 118(8): 3271–3277, https://doi.org/10.1002jgrd.50329

Appendix A

Table of Wavelength versus Ozone Absorption Coefficients

Multiply the appropriate coefficient by the columnar amount of ozone in atm-cm to find the ozone optical depth, τ_{ozone}. Note that one atm-cm is equal to DU/1000; recall that DU stands for Dobson Unit. For example, for a columnar amount of ozone of 300 DU, at 615 nm, τ_{ozone} = 300/1000*0.1162 = 0.03486.

Table 1. Wavelengths and ozone absorption coefficients.

λ	Ozone Absorption Coefficient	λ	Ozone Absorption Coefficient	λ	Ozone Absorption Coefficient	λ	Ozone Absorption Coefficient	λ	Ozone Absorption Coefficient
380	0.0000	381	0.0000	382	0.0000	383	0.0000	384	0.0000
385	0.0000	386	0.0000	387	0.0000	388	0.0000	389	0.0000
390	0.0000	391	0.0000	392	0.0000	393	0.0000	394	0.0000
395	0.0000	396	0.0000	397	0.0000	398	0.0000	399	0.0000
400	0.0000	401	0.0000	402	0.0000	403	0.0000	404	0.0000
405	0.0000	406	0.0000	407	0.0001	408	0.0002	409	0.0002
410	0.0003	411	0.0003	412	0.0003	413	0.0003	414	0.0003
415	0.0003	416	0.0004	417	0.0005	418	0.0005	419	0.0005
420	0.0005	421	0.0006	422	0.0007	423	0.0008	424	0.0010
425	0.0012	426	0.0013	427	0.0013	428	0.0013	429	0.0012
430	0.0012	431	0.0013	432	0.0015	433	0.0017	434	0.0017
435	0.0017	436	0.0017	437	0.0018	438	0.0021	439	0.0024
440	0.0029	441	0.0033	442	0.0037	443	0.0039	444	0.0040
445	0.0038	446	0.0036	447	0.0035	448	0.0035	449	0.0038
450	0.0042	451	0.0045	452	0.0046	453	0.0046	454	0.0046
455	0.0047	456	0.0052	457	0.0059	458	0.0069	459	0.0078
460	0.0087	461	0.0095	462	0.0098	463	0.0097	464	0.0092
465	0.0087	466	0.0084	467	0.0086	468	0.0092	469	0.0096
470	0.0101	471	0.0104	472	0.0105	473	0.0105	474	0.0108
475	0.0115	476	0.0127	477	0.0141	478	0.0158	479	0.0174
480	0.0193	481	0.0206	482	0.0215	483	0.0218	484	0.0213
485	0.0205	486	0.0200	487	0.0196	488	0.0197	489	0.0203
490	0.0213	491	0.0219	492	0.0223	493	0.0225	494	0.0230
495	0.0234	496	0.0244	497	0.0257	498	0.0274	499	0.0295
500	0.0320	501	0.0346	502	0.0372	503	0.0396	504	0.0414
505	0.0427	506	0.0431	507	0.0429	508	0.0423	509	0.0415
510	0.0409	511	0.0405	512	0.0410	513	0.0418	514	0.0428
515	0.0437	516	0.0446	517	0.0455	518	0.0463	519	0.0471
520	0.0481	521	0.0496	522	0.0511	523	0.0531	524	0.0554
525	0.0580	526	0.0605	527	0.0633	528	0.0659	529	0.0684

λ	Ozone Absorption Coefficient	λ	Ozone Absorption Coefficient	λ	Ozone Absorption Coefficient	λ	Ozone Absorption Coefficient	λ	Ozone Absorption Coefficient
530	0.0706	531	0.0725	532	0.0740	533	0.0749	534	0.0754
535	0.0755	536	0.0753	537	0.0753	538	0.0757	539	0.0764
540	0.0774	541	0.0787	542	0.0803	543	0.0819	544	0.0833
545	0.0846	546	0.0856	547	0.0866	548	0.0875	549	0.0882
550	0.0890	551	0.0899	552	0.0908	553	0.0918	554	0.0931
555	0.0944	556	0.0962	557	0.0981	558	0.1002	559	0.1027
560	0.1052	561	0.1078	562	0.1104	563	0.1128	564	0.1148
565	0.1166	566	0.1184	567	0.1199	568	0.1213	569	0.1229
570	0.1244	571	0.1257	572	0.1268	573	0.1275	574	0.1279
575	0.1278	576	0.1273	577	0.1264	578	0.1254	579	0.1243
580	0.1231	581	0.1219	582	0.1208	583	0.1197	584	0.1190
585	0.1184	586	0.1180	587	0.1179	588	0.1178	589	0.1180
590	0.1185	591	0.1196	592	0.1208	593	0.1226	594	0.1248
595	0.1270	596	0.1295	597	0.1318	598	0.1341	599	0.1360
600	0.1375	601	0.1384	602	0.1390	603	0.1388	604	0.1382
605	0.1371	606	0.1356	607	0.1337	608	0.1317	609	0.1294
610	0.1271	611	0.1248	612	0.1224	613	0.1203	614	0.1181
615	0.1162	616	0.1142	617	0.1124	618	0.1108	619	0.1092
620	0.1078	621	0.1065	622	0.1052	623	0.1039	624	0.1027
625	0.1014	626	0.1000	627	0.0987	628	0.0973	629	0.0957
630	0.0943	631	0.0929	632	0.0916	633	0.0901	634	0.0886
635	0.0870	636	0.0855	637	0.0839	638	0.0823	639	0.0807
640	0.0790	641	0.0775	642	0.0761	643	0.0747	644	0.0734
645	0.0720	646	0.0708	647	0.0696	648	0.0683	649	0.0673
650	0.0662	651	0.0652	652	0.0641	653	0.0630	654	0.0619
655	0.0608	656	0.0597	657	0.0586	658	0.0575	659	0.0565
660	0.0555	661	0.0546	662	0.0536	663	0.0526	664	0.0516
665	0.0505	666	0.0494	667	0.0482	668	0.0471	669	0.0460
670	0.0450	671	0.0440	672	0.0429	673	0.0419	674	0.0409
675	0.0401	676	0.0392	677	0.0383	678	0.0375	679	0.0368
680	0.0361	681	0.0355	682	0.0350	683	0.0345	684	0.0339
685	0.0333	686	0.0327	687	0.0320	688	0.0311	689	0.0303
690	0.0295	691	0.0287	692	0.0279	693	0.0273	694	0.0265
695	0.0258	696	0.0251	697	0.0244	698	0.0237	699	0.0232
700	0.0226	701	0.0221	702	0.0217	703	0.0212	704	0.0208
705	0.0205	706	0.0202	707	0.0199	708	0.0196	709	0.0193
710	0.0191	711	0.0189	712	0.0187	713	0.0185	714	0.0185
715	0.0183	716	0.0181	717	0.0177	718	0.0173	719	0.0168
720	0.0162	721	0.0156	722	0.0151	723	0.0147	724	0.0143
725	0.0140	726	0.0136	727	0.0134	728	0.0130	729	0.0126
730	0.0123	731	0.0120	732	0.0118	733	0.0116	734	0.0115
735	0.0114	736	0.0114	737	0.0113	738	0.0112	739	0.0112
740	0.0112	741	0.0113	742	0.0115	743	0.0116	744	0.0117
745	0.0118	746	0.0120	747	0.0119	748	0.0118	749	0.0116
750	0.0111	751	0.0106	752	0.0101	753	0.0096	754	0.0090

λ	Ozone Absorption Coefficient	λ	Ozone Absorption Coefficient	λ	Ozone Absorption Coefficient	λ	Ozone Absorption Coefficient	λ	Ozone Absorption Coefficient
755	0.0086	756	0.0082	757	0.0079	758	0.0077	759	0.0075
760	0.0073	761	0.0072	762	0.0070	763	0.0070	764	0.0070
765	0.0069	766	0.0068	767	0.0067	768	0.0067	769	0.0068
770	0.0068	771	0.0069	772	0.0071	773	0.0072	774	0.0075
775	0.0079	776	0.0081	777	0.0083	778	0.0084	779	0.0085
780	0.0084	781	0.0082	782	0.0079	783	0.0075	784	0.0071
785	0.0067	786	0.0063	787	0.0061	788	0.0058	789	0.0056
790	0.0054	791	0.0052	792	0.0049	793	0.0047	794	0.0046
795	0.0044	796	0.0043	797	0.0042	798	0.0042	799	0.0041
800	0.0040	801	0.0040	802	0.0040	803	0.0039	804	0.0040
805	0.0040	806	0.0041	807	0.0042	808	0.0044	809	0.0046
810	0.0048	811	0.0050	812	0.0052	813	0.0054	814	0.0056
815	0.0057	816	0.0057	817	0.0057	818	0.0056	819	0.0055
820	0.0052	821	0.0049	822	0.0046	823	0.0043	824	0.0040
825	0.0037	826	0.0034	827	0.0031	828	0.0029	829	0.0027
830	0.0025	831	0.0024	832	0.0023	833	0.0022	834	0.0021
835	0.0021	836	0.0020	837	0.0020	838	0.0020	839	0.0020
840	0.0020	841	0.0020	842	0.0021	843	0.0021	844	0.0022
845	0.0023	846	0.0024	847	0.0026	848	0.0028	849	0.0030
850	0.0032	851	0.0035	852	0.0037	853	0.0038	854	0.0038
855	0.0037	856	0.0036	857	0.0035	858	0.0033	859	0.0032
860	0.0029	861	0.0027	862	0.0025	863	0.0023	864	0.0021
865	0.0019	866	0.0017	867	0.0016	868	0.0015	869	0.0014
870	0.0013	871	0.0013	872	0.0012	873	0.0011	874	0.0011
875	0.0011	876	0.0010	877	0.0010	878	0.0010	879	0.0010
880	0.0011	881	0.0011	882	0.0011	883	0.0011	884	0.0012
885	0.0012	886	0.0013	887	0.0013	888	0.0013	889	0.0014
890	0.0014	891	0.0013	892	0.0013	893	0.0014	894	0.0014
895	0.0015	896	0.0016	897	0.0016	898	0.0017	899	0.0017
900	0.0016	901	0.0015	902	0.0014	903	0.0014	904	0.0013
905	0.0012	906	0.0011	907	0.0010	908	0.0009	909	0.0009
910	0.0008	911	0.0007	912	0.0007	913	0.0006	914	0.0006
915	0.0005	916	0.0005	917	0.0005	918	0.0005	919	0.0005
920	0.0005	921	0.0004	922	0.0004	923	0.0004	924	0.0004
925	0.0004	926	0.0004	927	0.0004	928	0.0004	929	0.0004
930	0.0004	931	0.0004	932	0.0004	933	0.0004	934	0.0004
935	0.0005	936	0.0005	937	0.0005	938	0.0006	939	0.0007
940	0.0008	941	0.0009	942	0.0010	943	0.0011	944	0.0011
945	0.0011	946	0.0010	947	0.0009	948	0.0008	949	0.0007
950	0.0007	951	0.0006	952	0.0005	953	0.0005	954	0.0004
955	0.0004	956	0.0004	957	0.0004	958	0.0003	959	0.0003
960	0.0003	961	0.0000	962	0.0000	963	0.0000	964	0.0000
965	0.0000	966	0.0000	967	0.0000	968	0.0000	969	0.0000
970	0.0000	971	0.0000	972	0.0000	973	0.0000	974	0.0000
975	0.0000								

Appendix B

Contents of netCDF Output for the AOD VAP

In the ARM Data Center, these files are given names such as "sgpmfrsraod1michE13.c1.20101001.000000.cdf".

Table 2. netCDF output for the AOD VAP.

Variable	Units
base_time	seconds since 1/1/1970 0:00:00
time_offset	seconds since 4/29/1997 0:00:00
time	seconds since 4/29/1997 0:00:00
qc_time	unitless
hemisp_broadband_raw	counts
qc_hemisp_broadband_raw	unitless
hemisp_narrowband_filter1_raw	counts
qc_hemisp_narrowband_filter1_raw	unitless
hemisp_narrowband_filter2_raw	counts
qc_hemisp_narrowband_filter2_raw	unitless
hemisp_narrowband_filter3_raw	counts
qc_hemisp_narrowband_filter3_raw	unitless
hemisp_narrowband_filter4_raw	counts
qc_hemisp_narrowband_filter4_raw	unitless
hemisp_narrowband_filter5_raw	counts
qc_hemisp_narrowband_filter5_raw	unitless
hemisp_narrowband_filter6_raw	counts
qc_hemisp_narrowband_filter6_raw	unitless
diffuse_hemisp_broadband_raw	counts
qc_diffuse_hemisp_broadband_raw	unitless
diffuse_hemisp_narrowband_filter1_raw	counts
qc_diffuse_hemisp_narrowband_filter1_raw	unitless
diffuse_hemisp_narrowband_filter2_raw	counts
qc_diffuse_hemisp_narrowband_filter2_raw	unitless
diffuse_hemisp_narrowband_filter3_raw	counts
qc_diffuse_hemisp_narrowband_filter3_raw	unitless
diffuse_hemisp_narrowband_filter4_raw	counts
qc_diffuse_hemisp_narrowband_filter4_raw	unitless
diffuse_hemisp_narrowband_filter5_raw	counts
qc_diffuse_hemisp_narrowband_filter5_raw	unitless
diffuse_hemisp_narrowband_filter6_raw	counts
qc_diffuse_hemisp_narrowband_filter6_raw	unitless
hemisp_broadband	W/m^2

Variable	Units
qc_hemisp_broadband	unitless
hemisp_narrowband_filter1	W/m^2/nm
qc_hemisp_narrowband_filter1	unitless
hemisp_narrowband_filter2	W/m^2/nm
qc_hemisp_narrowband_filter2	unitless
hemisp_narrowband_filter3	W/m^2/nm
qc_hemisp_narrowband_filter3	unitless
hemisp_narrowband_filter4	W/m^2/nm
qc_hemisp_narrowband_filter4	unitless
hemisp_narrowband_filter5	W/m^2/nm
qc_hemisp_narrowband_filter5	unitless
hemisp_narrowband_filter6	W/m^2/nm
qc_hemisp_narrowband_filter6	unitless
diffuse_hemisp_broadband	W/m^2
qc_diffuse_hemisp_broadband	unitless
diffuse_hemisp_narrowband_filter1	W/m^2/nm
qc_diffuse_hemisp_narrowband_filter1	unitless
diffuse_hemisp_narrowband_filter2	W/m^2/nm
qc_diffuse_hemisp_narrowband_filter2	unitless
diffuse_hemisp_narrowband_filter3	W/m^2/nm
qc_diffuse_hemisp_narrowband_filter3	unitless
diffuse_hemisp_narrowband_filter4	W/m^2/nm
qc_diffuse_hemisp_narrowband_filter4	unitless
diffuse_hemisp_narrowband_filter5	W/m^2/nm
qc_diffuse_hemisp_narrowband_filter5	unitless
diffuse_hemisp_narrowband_filter6	W/m^2/nm
qc_diffuse_hemisp_narrowband_filter6	unitless
direct_normal_broadband	W/m^2
qc_direct_normal_broadband	unitless
direct_normal_narrowband_filter1	W/m^2/nm
qc_direct_normal_narrowband_filter1	unitless
direct_normal_narrowband_filter2	W/m^2/nm
qc_direct_normal_narrowband_filter2	unitless
direct_normal_narrowband_filter3	W/m^2/nm
qc_direct_normal_narrowband_filter3	unitless
direct_normal_narrowband_filter4	W/m^2/nm
qc_direct_normal_narrowband_filter4	unitless
direct_normal_narrowband_filter5	W/m^2/nm
qc_direct_normal_narrowband_filter5	unitless
direct_normal_narrowband_filter6	W/m^2/nm
qc_direct_normal_narrowband_filter6	unitless
alltime_hemisp_broadband	counts
qc_alltime_hemisp_broadband	unitless
alltime_hemisp_narrowband_filter1	counts
qc_alltime_hemisp_narrowband_filter1	unitless

Variable	Units
alltime_hemisp_narrowband_filter2	counts
qc_alltime_hemisp_narrowband_filter2	unitless
alltime_hemisp_narrowband_filter3	counts
qc_alltime_hemisp_narrowband_filter3	unitless
alltime_hemisp_narrowband_filter4	counts
qc_alltime_hemisp_narrowband_filter4	unitless
alltime_hemisp_narrowband_filter5	counts
qc_alltime_hemisp_narrowband_filter5	unitless
alltime_hemisp_narrowband_filter6	counts
qc_alltime_hemisp_narrowband_filter6	unitless
direct_horizontal_broadband	W/m^2
qc_direct_horizontal_broadband	unitless
direct_horizontal_narrowband_filter1	W/m^2/nm
qc_direct_horizontal_narrowband_filter1	unitless
direct_horizontal_narrowband_filter2	W/m^2/nm
qc_direct_horizontal_narrowband_filter2	unitless
direct_horizontal_narrowband_filter3	W/m^2/nm
qc_direct_horizontal_narrowband_filter3	unitless
direct_horizontal_narrowband_filter4	W/m^2/nm
qc_direct_horizontal_narrowband_filter4	unitless
direct_horizontal_narrowband_filter5	W/m^2/nm
qc_direct_horizontal_narrowband_filter5	unitless
direct_horizontal_narrowband_filter6	W/m^2/nm
qc_direct_horizontal_narrowband_filter6	unitless
direct_diffuse_ratio_broadband	unitless
qc_direct_diffuse_ratio_broadband	unitless
direct_diffuse_ratio_filter1	unitless
qc_direct_diffuse_ratio_filter1	unitless
direct_diffuse_ratio_filter2	unitless
qc_direct_diffuse_ratio_filter2	unitless
direct_diffuse_ratio_filter3	unitless
qc_direct_diffuse_ratio_filter3	unitless
direct_diffuse_ratio_filter4	unitless
qc_direct_diffuse_ratio_filter4	unitless
direct_diffuse_ratio_filter5	unitless
qc_direct_diffuse_ratio_filter5	unitless
direct_diffuse_ratio_filter6	unitless
qc_direct_diffuse_ratio_filter6	unitless
head_temp	degrees C
qc_head_temp	unitless
head_temp2	degrees C
qc_head_temp2	unitless
logger_temp	degrees C
qc_logger_temp	unitless
logger_volt	volts

Variable	Units
qc_logger_volt	unitless
solar_zenith_angle	degrees
cosine_solar_zenith_angle	unitless
elevation_angle	degrees
airmass	unitless
qc_airmass	unitless
azimuth_angle	degrees
computed_cosine_correction_broadband	unitless
qc_computed_cosine_correction_broadband	unitless
computed_cosine_correction_filter1	unitless
qc_computed_cosine_correction_filter1	unitless
computed_cosine_correction_filter2	unitless
qc_computed_cosine_correction_filter2	unitless
computed_cosine_correction_filter3	unitless
qc_computed_cosine_correction_filter3	unitless
computed_cosine_correction_filter4	unitless
qc_computed_cosine_correction_filter4	unitless
computed_cosine_correction_filter5	unitless
qc_computed_cosine_correction_filter5	unitless
computed_cosine_correction_filter6	unitless
qc_computed_cosine_correction_filter6	unitless
bench_angle	(bench_angle) degress
cosine_correction_sn_broadband	(bench angle) unitless
cosine_correction_sn_filter1	(bench angle) unitless
cosine_correction_sn_filter2	(bench angle) unitless
cosine_correction_sn_filter3	(bench angle) unitless
cosine_correction_sn_filter4	(bench angle) unitless
cosine_correction_sn_filter5	(bench angle) unitless
cosine_correction_sn_filter6	(bench angle) unitless
cosine_correction_we_broadband	(bench angle) unitless
cosine_correction_we_filter1	(bench angle) unitless
cosine_correction_we_filter2	(bench angle) unitless
cosine_correction_we_filter3	(bench angle) unitless
cosine_correction_we_filter4	(bench angle) unitless
cosine_correction_we_filter5	(bench angle) unitless
cosine_correction_we_filter6	(bench angle) unitless
wavelength_filter1	(wavelength) nm
qc_wavelength_filter1	(wavelength) unitless
normalized_transmittance_filter1	(wavelength) unitless
qc_normalized_transmittance_filter1	(wavelength) unitless
wavelength_filter2	(wavelength) nm
qc_wavelength_filter2	(wavelength) unitless
normalized_transmittance_filter2	(wavelength) unitless
qc_normalized_transmittance_filter2	(wavelength) unitless
wavelength_filter3	(wavelength) nm

Variable	Units
qc_wavelength_filter3	(wavelength) unitless
normalized_transmittance_filter3	(wavelength) unitless
qc_normalized_transmittance_filter3	(wavelength) unitless
wavelength_filter4	(wavelength) nm
qc_wavelength_filter4	(wavelength) unitless
normalized_transmittance_filter4	(wavelength) unitless
qc_normalized_transmittance_filter4	(wavelength) unitless
wavelength_filter5	(wavelength) nm
qc_wavelength_filter5	(wavelength) unitless
normalized_transmittance_filter5	(wavelength) unitless
qc_normalized_transmittance_filter5	(wavelength) unitless
wavelength_filter6	(wavelength) nm
qc_wavelength_filter6	(wavelength) unitless
normalized_transmittance_filter6	(wavelength) unitless
qc_normalized_transmittance_filter6	(wavelength) unitless
wavelength	(wavelength) nm
TOA_irradiance	(wavelength) W/m^2/nm
offset_broadband	counts
offset_filter1	counts
offset_filter2	counts
offset_filter3	counts
offset_filter4	counts
offset_filter5	counts
offset_filter6	counts
diffuse_correction_broadband	unitless
diffuse_correction_filter1	unitless
diffuse_correction_filter2	unitless
diffuse_correction_filter3	unitless
diffuse_correction_filter4	unitless
diffuse_correction_filter5	unitless
diffuse_correction_filter6	unitless
nominal_calibration_factor_broadband	count/(W/m^2)
nominal_calibration_factor_filter1	count/(W/m^2/nm)
nominal_calibration_factor_filter2	count/(W/m^2/nm)
nominal_calibration_factor_filter3	count/(W/m^2/nm)
nominal_calibration_factor_filter4	count/(W/m^2/nm)
nominal_calibration_factor_filter5	count/(W/m^2/nm)
nominal_calibration_factor_filter6	count/(W/m^2/nm)
total_optical_depth_filter1	unitless
qc_total_optical_depth_filter1	unitless
total_optical_depth_filter2	unitless
qc_total_optical_depth_filter2	unitless
total_optical_depth_filter3	unitless
qc_total_optical_depth_filter3	unitless
total_optical_depth_filter4	unitless

Variable	Units
qc_total_optical_depth_filter4	unitless
total_optical_depth_filter5	unitless
qc_total_optical_depth_filter5	unitless
angstrom_exponent	unitless
qc_angstrom_exponent	unitless
aerosol_optical_depth_filter1	unitless
qc_aerosol_optical_depth_filter1	unitless
aerosol_optical_depth_filter2	unitless
qc_aerosol_optical_depth_filter2	unitless
aerosol_optical_depth_filter3	unitless
qc_aerosol_optical_depth_filter3	unitless
aerosol_optical_depth_filter4	unitless
qc_aerosol_optical_depth_filter4	unitless
aerosol_optical_depth_filter5	unitless
qc_aerosol_optical_depth_filter5	unitless
variability_flag	unitless
surface_pressure	kPa
Io_filter1	W/m^2/nm
qc_Io_filter1	unitless
Io_filter2	W/m^2/nm
qc_Io_filter2	unitless
Io_filter3	W/m^2/nm
qc_Io_filter3	unitless
Io_filter4	W/m^2/nm
qc_Io_filter4	unitless
Io_filter5	W/m^2/nm
qc_Io_filter5	unitless
Ozone_column_amount	Dobson Units
qc_Ozone_column_amount	unitless
Rayleigh_optical_depth_filter1	unitless
Rayleigh_optical_depth_filter2	unitless
Rayleigh_optical_depth_filter3	unitless
Rayleigh_optical_depth_filter4	unitless
Rayleigh_optical_depth_filter5	unitless
Ozone_optical_depth_filter1	unitless
Ozone_optical_depth_filter2	unitless
Ozone_optical_depth_filter3	unitless
Ozone_optical_depth_filter4	unitless
Ozone_optical_depth_filter5	unitless
sun_to_earth_distance	AU
lat	degree_N
lon	degree_E
alt	m

www.arm.gov

U.S. DEPARTMENT OF
ENERGY

Office of Science